Received: 23 November 2020 | Revised: 17 February 2021 | Accepted: 24 February 2021

DOI: 10.1002/glia.23987

GLIA

WILEY

RESEARCH ARTICLE

Astrocyte glutamate uptake coordinates experience-dependent, eye-specific refinement in developing visual cortex

Grayson O. Sipe[1] | Jeremy Petravicz[1] | Rajeev V. Rikhye[1] | Rodrigo Garcia[1] | Nikolaos Mellios[2,3] | Mriganka Sur[1]

[1]Department of Brain and Cognitive Sciences, Picower Institute of Learning and Memory, Massachusetts Institute of Technology, Cambridge, Massachusetts

[2]Department of Neurosciences, University of New Mexico School of Medicine, Albuquerque, New Mexico

[3]Autophagy Inflammation and Metabolism (AIM) Center, Albuquerque, New Mexico

Correspondence
Mriganka Sur, Department of Brain and Cognitive Sciences, Picower Institute of Learning and Memory, Massachusetts Institute of Technology, Cambridge, MA 02139, USA.
Email: msur@mit.edu

Funding information
National Eye Institute, Grant/Award Numbers: 1F32EY022264, 1F32EY028028, R01EY028219; National Institute on Drug Abuse, Grant/Award Number: R01DA049005

Abstract

The uptake of glutamate by astrocytes actively shapes synaptic transmission, however its role in the development and plasticity of neuronal circuits remains poorly understood. The astrocytic glutamate transporter, GLT1 is the predominant source of glutamate clearance in the adult mouse cortex. Here, we examined the structural and functional development of the visual cortex in GLT1 heterozygous (HET) mice using two-photon microscopy, immunohistochemistry and slice electrophysiology. We find that though eye-specific thalamic axonal segregation is intact, binocular refinement in the primary visual cortex is disrupted. Eye-specific responses to visual stimuli in GLT1 HET mice show altered binocular matching, with abnormally high responses to ipsilateral compared to contralateral eye stimulation and a greater mismatch between preferred orientation selectivity of ipsilateral and contralateral eye responses. Furthermore, we observe an increase in dendritic spine density in the basal dendrites of layer 2/3 excitatory neurons suggesting aberrant spine pruning. Monocular deprivation induces atypical ocular dominance plasticity in GLT1 HET mice, with an unusual depression of ipsilateral open eye responses; however, this change in ipsilateral responses correlates well with an upregulation of GLT1 protein following monocular deprivation. These results demonstrate that a key function of astrocytic GLT1 function during development is the experience-dependent refinement of ipsilateral eye inputs relative to contralateral eye inputs in visual cortex.

KEYWORDS
astrocytes, glutamate uptake, visual cortex development

1 | INTRODUCTION

Astrocytes constitute a major class of cells in the mammalian brain with critical roles in brain homeostasis, function, and plasticity (Verkhratsky & Nedergaard, 2018). However, the role of astrocytes in cortical development and plasticity remains poorly understood. Astrocyte processes are known to form intimate contacts with neuronal synapses ensheathing sites of neurotransmitter release and regulating synaptic efficacy and plasticity (Araque et al., 2014; Durkee & Araque, 2019; Eroglu & Barres, 2010; Papouin, Dunphy, Tolman, Foley, & Haydon, 2017). Furthermore, astrocytes are the primary cell type responsible for clearance of synaptic glutamate via excitatory amino acid transporters (EAATs) (Aida et al., 2015; Danbolt, 2001; Petr et al., 2015). Neuronal excitability and synaptic transmission are modulated by the expression of EAATs in numerous brain regions including the cortex (Campbell & Hablitz, 2004), thalamus (Hauser, Edson, Hooks, & Chen, 2013), spinal cord (Weng, Chen, Pan, & Nie, 2007), cerebellum (Takatsuru, Iino, Tanaka, & Ozawa, 2007), striatum (Pinky, Wilkie, Barnes, & Parsons, 2018), and hippocampus (Huang, Sinha, Tanaka, Rothstein, & Bergles, 2004). Astrocytes express two EAATs, GLAST (EAAT1) and GLT1 (EAAT2) with varying regional expression during development to adulthood (Danbolt, 2001; Hanson

Grayson O. Sipe and Jeremy Petravicz contributed equally to this work.

et al., 2015; Pinky et al., 2018). In the adult mouse cortex, GLT1 is responsible for approximately 80–90% of synaptic glutamate clearance, thereby representing a critical mechanism for modulating synaptic transmission and function (Danbolt, 2001). In addition, the dynamic ensheathment of synapses by astrocyte processes (Perez-Alvarez, Navarrete, Covelo, Martin, & Araque, 2014), the modulation of GLT1 expression by increased network activity (Genoud et al., 2006; Murphy-Royal et al., 2015), and the subcellular trafficking of GLT1 to highly active synaptic zones (Benediktsson et al., 2012) together suggest that GLT1 serves a critical role in astrocyte-neuron signaling so as to facilitate synaptic plasticity through dynamic glutamate uptake commensurate with synaptic strength. As such, disruptions in GLT1 expression or function have been implicated in several neuropathologies (Cui et al., 2014; Robinson, Lee, & DaSilva, 2020; Sugimoto et al., 2018). Previous work with GLT1 knockout mice has provided evidence that GLT1 expression is crucial for early postnatal development of many brain regions (Matsugami et al., 2006) and also in plasticity in the developing somatosensory cortex (Takasaki et al., 2008).

The mouse primary visual cortex (V1) has served as a useful model system for studying cortical development and plasticity (Hensch, 2005; Hooks & Chen, 2020; Leamey, Van Wart, & Sur, 2009; Schummers, Sharma, & Sur, 2005). Layer 2/3 excitatory neurons in the binocular region of V1 receive information from both the contralateral and ipsilateral eye via thalamocortical and intracortical inputs that are shaped during critical periods of experience-dependent plasticity (Hooks & Chen, 2020). The matching of binocular orientation preference, in which neurons receiving binocular input alter their synaptic connections to align the orientation preference of both contralateral and ipsilateral eye responses, represents one key example of experience-dependent plasticity (Antonini, Fagiolini, & Stryker, 1999; Bhaumik & Shah, 2014; Gu & Cang, 2016; Kara & Boyd, 2009; Tie et al., 2018; Wang, Sarnaik, & Cang, 2010). This refinement of binocular matching is dependent upon NMDA receptors acting as coincidence detectors of contra- and ipsilateral drive (Sawtell et al., 2003), and NMDA receptor stimulation is known to be affected by loss of GLT1 function (Aida et al., 2015; Aida, Ito, Takahashi, & Tanaka, 2012; Pinky et al., 2018). In addition, the anatomical and synaptic inputs onto binocular V1 neurons are weighted such that there is normally a contralateral eye bias in response amplitude (Antonini et al., 1999). Monocular deprivation (MD) of the contralateral eye for a few days (between ~P21 and 30) leads to decreased contralateral eye responses followed by a homeostatic increase in ipsilateral eye responses (Hensch, 2005; Hooks & Chen, 2020). This process is termed ocular dominance plasticity (ODP) and defines a second type of experience dependent plasticity in V1 (Espinosa & Stryker, 2012; Katz & Crowley, 2002; Trachtenberg, 2015).

In order to explore astrocytic roles in development via GLT1-mediated glutamate uptake, we characterized the developmental timeline of GLT1 expression and used a transgenic mouse line with constitutive heterozygous expression of the GLT1 gene (SLC1A2, GLT1-HET; Kiryk et al., 2008) to examine the consequences of decreased astrocyte glutamate uptake in visual cortex development. Our data show that GLT1 heterozygosity results in disrupted binocular matching, abnormal excitation/inhibition, and aberrant ODP. Interestingly, large-scale synaptic remodeling induced by monocular deprivation causes a haplosufficient increase in GLT1 expression and blocks ipsilateral eye response potentiation, indicating that the ipsilateral inputs are particularly sensitive to astrocyte-mediated glutamate uptake. This work demonstrates an important and unexpected role for astrocytic glutamate uptake in the development and experience-dependent plasticity of eye-specific responses in V1.

2 | METHODS

2.1 | Animals and surgery

GLT1-HET mice on a C57/Bl6 background were obtained from Kohichi Tanaka and Jeffrey Rothstein, and maintained in their home cage until experiments under a 12/12 light/dark cycle with food and standard mouse chow provided ad libitum. GLT1 HET mice were also crossed with Thy-GFP mice (Jackson Labs) and GFAP-tDTomato mice to analyze neuronal and astrocyte morphology respectively. Male and female mice were used throughout the study with GLT1 WT littermates as controls. For in vivo imaging of neurons, GLT1 HET mice were crossed to Emx-Cre::GCaMP6f mice (Jackson Labs) to allow for imaging of neuronal responses in the binocular region of the visual cortex at P30-32. At age P24-25, mice were anesthetized using isoflurane (3% induction, 1.5–2% during surgery). A 3-mm-diameter craniotomy was performed over binocular V1 (2–3 mm lateral and 0.5 mm anterior to lambda). The craniotomy was covered with a 3 mm glass coverslip (Warner Instruments), and a custom-built metal head post was attached to the skull and sealed with dental cement (C&B-Metabond, Parkell). Care was taken not to rupture the dura mater. The core body temperature was maintained at 37.5°C using a heating blanket (Harvard Apparatus). For ocular dominance plasticity (ODP) experiments, MD was performed by eyelid suture. Animals (~P21–24) were anesthetized with isoflurane (3% induction, 1.5–2% during surgery), and eyelid margins trimmed. Upper and lower lids were sutured closed, and eyelids were regularly examined to ensure that they remained closed for the duration of the experiment. MD lasted either 4 or 7 days according to established models of short and long-term ODP (Hooks & Chen, 2020; Nagakura, Van Wart, Petravicz, Tropea, & Sur, 2014). Before optical imaging, the sutures were removed and the deprived eye reopened while the animal was under anesthesia. All animal procedures were performed in strict accordance with protocols established with the Massachusetts Institute of Technology, Division of Comparative Medicine, and conformed to NIH guidelines.

2.2 | Immunohistochemistry

Mice were deeply anesthetized using isoflurane and transcardially perfused with 0.1 M phosphate buffered saline (PBS) and 4% paraformaldehyde in PBS. Whole brains were removed and post-fixed overnight at 4°C until sectioning. Coronal brain slices were acquired at a thickness of 40 μm using a vibratome (VT1200S; Leica) and stained or

directly slide-mounted with general purpose mounting media with DAPI (Vector Labs). Free-floating brain slices were washed (3 ×10 min @ ~20°C, 0.1 M PBS) and then blocked (1 hr at ~20°C; 5% BSA/1% triton in wash buffer). Immediately following blocking, tissue was incubated in primary antibody solution (24 hr at ~4°C; 3% BSA/0.1% triton in wash buffer), washed (3 × 10min) and placed in secondary antibody solution (4 hr at ~20°C, 3% BSA/0.1% triton in wash buffer). Tissue was then washed (3 × 10 min) and mounted on to microscope slides as described above. The following primary antibodies and dilutions were used: rabbit α-GLT1 (1:500, AGC-022, Alamone Labs), guinea pig α-GFAP (1:2000, 173 004, Synaptic Systems), chicken α-GFP (1:1000, GFP-1020, Aves Labs). The following secondary antibodies and dilutions were used (1:500, AlexaFluor, Invitrogen): goat α-rabbit, goat α-chicken and goat anti-guinea pig.

2.3 | mRNA and protein quantification

For quantification of GLT1 mRNA, mouse RNA from V1 was extracted using the miRNeasy Mini Kit (Qiagen) based on manufacturer's instructions. RNA concentration and quality was assayed using NanoDrop (Thermo Scientific) and 300 ng of RNA were reverse transcribed using the Vilo cDNA kit (Invitrogen) with a 1:15 dilution of cDNA. GLT1 mRNA was normalized to β-actin using the following formula: GLT1 relative expression = $2^{CT^{\beta\text{-actin}}}/2^{CT^{GLT1}}$ mRNA. For protein measurements of GLT1 and GLAST, V1 contralateral to the deprived eye was removed and snap-frozen with dry ice. The brains were homogenized in RIPA buffer (Invitrogen) containing proteinase and phosphatase inhibitors (Roche), centrifuged for 10 min at 8,000 × g at 4°C and supernatant extracted and stored at -80°C. Protein concentration was assayed using BCA protein assays (Pierce, Thermo Scientific). For Western blot, 10 μg/μl of protein was loaded into each lane of 4–15% (mg/100 mL) Tris·HCl polyacryamide gels (Bio-Rad). Protein was transferred to Immobilon-P PVDF membranes (Millipore), blocked with 5% (mg/100 mL) BSA (Sigma) for 1 hr, and incubated in the following antibody solutions overnight: GLT1 (1:25k, AB1783, EMD Millipore), GLAST (1:10k, ab181036, Abcam), and β-actin (1:20k, A1978; Sigma-Aldrich). Blots were then incubated in the following horseradish peroxidase-conjugated secondary antibodies (IRDye® 800CW Donkey anti-Rabbit IgG, Licor System) for 1.5 hr, washed and then imaged. Optical densities of detected bands were quantified using ImageJ software. A standard sample of wild-type mouse V1 tissue was run on each gel to gauge blot-to-blot variability.

2.4 | Labeling of retinal ganglion axons

GLT1 HET and WT mice (~P28-P32) were anesthetized with isoflurane, and 2 μL of cholera toxin subunit B (CTB) conjugated to Alexa Fluor 488 was injected into the ipsilateral eye and Alexa Fluor 594 into the contralateral eye (1 mg/mL; Invitrogen). After 6 days, animals were perfused and prepared as described above. Projection overlap was quantified in ImageJ as previously described (Ip et al., 2018; Nagakura et al., 2014; Stevens et al., 2007).

2.5 | Two-photon imaging

Two-photon in vivo imaging was performed in awake, head-fixed mice as described previously (Rikhye & Sur, 2015). Images of GCaMP6f-positive neurons were obtained using a Prairie Ultima two-photon system (Bruker) driven by a Spectra Physics Mai-Tai laser passed through a Deep-See module (Spectra Physics) and a high-performance objective lens (25 Olympus XL Plan Nobjective, 1.05 numerical aperture). Cells were excited at 910 nm for GCaMP6f. A custom-built MATLAB-based (MathWorks) software system was used to collect optimized raster scans at 20 Hz. The binocular region of V1 was determined by covering the eye contralateral to the craniotomy with an eye patch, and neuronal responses elicited by displaying moving gratings. If neuronal responses were visually detected, responses were confirmed using the contralateral eye while the ipsilateral eye was covered. Fields where neuronal responses were detected to both contra- and ipsilateral stimulation were used in experiments. Single eye responses to orientated gratings were then collected from each field. To assess the orientation selectivity and tuning of neurons, we presented oriented gratings on a 23″ 1080p LCD monitor (Dell) using custom software (Network Visstim, Sur Lab) written in PsychToolbox-3 (Psychtoolbox.com) on a Windows 10 computer (Dell Precision) with a GeForce 8800 GTS 640 MB graphics card (PNY). Gratings were optimized for cellular responsiveness using a contrast of 100%, spatial frequency of 0.002–0.256 cycles/°, and a temporal frequency of 1–3 Hz. Gratings were presented by stepping the orientation from 0 to 360° in steps of 30°, with each grating presentation being preceded for 4 s "off" followed by 2 s "on."

Cells were selected for analysis based on the OSI (orientation selectivity index) and tuning curve fits. Tuning curve fits were computed for the tuning curves using a sum of two Gaussians with peaks 180° apart and five parameters: preferred orientation, θp; tuning width, σ (shared by the two directions); baseline response, R0; response at the preferred orientation, Rp; and response at the null orientation, Rn. Optimal parameters were determined with least-squares fit using MATLAB's *lsqnonlin* routine. Goodness of fit was determined from the R^2. Cells with $R^2 > 0.50$ were included for further analysis. For quantitative tuning analyses, the OSI was computed by taking the vector average of responses to all orientations, according to the formula described previously (Banerjee et al., 2016):

$$OSI = \frac{\sqrt{\left(\sum_i R(\theta_i)\sin(2\theta_i)\right)^2 + \left(\sum_i R(\theta_i)\cos(2\theta_i)\right)^2}}{\sum_i R(\theta_i)}$$

Cells were filtered based on visual responsiveness (*t*-test, OFF vs. ON, $p < 0.05$) and selectivity (OSI >0.15).

2.6 | Slice electrophysiology

Mice were anesthetized with isoflurane and the brain was rapidly removed and sliced coronally using a vibratome (VT1200S; Leica) at a

thickness of 300 μm in slicing buffer (mM: 130 choline chloride, 25 glucose, 1.25 NaH_2PO_4, 26 $NaCHO_3$, 2.5 KCl, 7 $MgCl_2$, and 0.5 $CaCl_2$) bubbled with 95% O_2 and 5% CO_2. Slices were incubated for a minimum of 60 min in room-temperature ACSF (mM: 130 NaCl, 10 glucose, 1.25 NaH_2PO_4, 24 $NaCHO_3$, 3.5 KCl, 2.5 $CaCl_2$, and 1.5 $MgCl_2$). For recording of AMPA receptor (AMPAR)-mediated mEPSCs, whole-cell patch clamp of layer II/III pyramidal neurons in the binocular region of V1 was performed using pipettes (4–7 MΩ resistance) filled with an internal solution (mM: 100 K-gluconate, 20 KCl, 0.5 EGTA, 10 NaCl, 10 Na-phosphocreatine, 4 Mg-ATP, 0.3 Na-GTP, and 10 HEPES, pH 7.2–7.3 titrated with 1 M KOH). Neurons were recorded at room temperature (25°C) in ACSF containing 1 μM TTX, 50 μM AP-5, and 50 μM picrotoxin to isolate AMPAR-mediated currents and voltage clamped at a membrane potential of −70 mV. mEPSCs were recorded using a Multiclamp 700B amplifier (Molecular Devices) at 10 kHz, filtered at 2 kHz, and analyzed with Clampfit 10.2 software (Molecular Devices). Whole-cell membrane currents were recorded for 10 min. For detection of mEPSCs, a detection template for each cell was constructed from four to six events intrinsic to each recording. Traces were analyzed in template search mode in Clampfit 10.2, with a template match threshold of 4–4.5 to reduce false positives. All events were detected automatically and edited after detection by eye to remove events that were erroneous matches or duplicate events. All mEPSC events were included in the analysis of event parameters.

2.7 | Intrinsic signal optical imaging

Mice were anesthetized with urethane (1.5 mg/g, i.p.) and chloroprothixene (10 mg/kg, i.p.). The skull was exposed over V1 and a head plate fixed to the head and minimize movements. The cortex was covered with agarose solution (1.5%) and a glass coverslip. Red light (630 nm) was used to illuminate the cortical surface, and the change of luminance was captured by a CCD camera (Cascade 512B; Roper Scientific) during the presentation of visual stimuli (custom MATLAB scripts). An elongated horizontal white bar (9° × 72°) over a uniformly gray background was drifted upward continuously through the peripheral-central dimension of the visual field. After moving to the last position, the bar would jump back to the initial position and start another cycle of movement; thus, the chosen region of visual space (72° × 72°) was stimulated in a periodic manner (12 s/cycle). Images of the visual cortex were continuously captured at the rate of 18 frames/s during each stimulus session of 22 min. A temporal high-pass filter (135 frames) was used to remove slow noise components, after which the temporal fast Fourier transform (FFT) component at the stimulus frequency (9 s^{-1}) was calculated pixel by pixel from the entire set of images. The amplitude of the FFT component was used to measure the strength of visually driven response for each eye, and the OD index (ODI) was derived from the response of each eye (R) at each pixel as ODI = $(R_{contra} - R_{ipsi})/(R_{contra} + R_{ipsi})$. The binocular zone was defined as the cortical region that was driven by stimulation of both the ipsilateral and contralateral eyes. The response amplitude for each eye was defined as fractional changes in reflectance over baseline reflectance ($\Delta R/R \times 10^{-3}$), and the top 50% pixels were analyzed to avoid background contamination.

2.8 | Statistical analyses

Two-tailed unpaired Student's *t*-tests were used for comparisons between two means. For comparing more than two means, a one-way or two-way analysis of variance (ANOVA) was used as appropriate followed by post-hoc pairwise comparisons using the Holm–Sidak method. Individual data points plotted represent averages from separate animals. All statistical tests were performed using Prism (GraphPad, La Jolla). All averaged data are presented as mean ± SEM.

3 | RESULTS

3.1 | GLT1 expression in the visual cortex during development

We first confirmed that GLT1 is expressed in the visual cortex during the critical period for ocular dominance plasticity (∼P28) when activity driven synaptic refinement is particularly prominent. Indeed, we found that GLT1 protein was highly expressed across all cortical layers (Figure 1a,b) as previously reported (Massie et al., 2003; Voutsinos-Porche et al., 2003). Next, we asked whether GLT1 transcription changed during a period of eye-specific refinement and binocular matching in V1. GLT1 mRNA transcripts were collected from visual cortex from P0–P60 and normalized to P28 to determine whether GLT1 transcription correlated with eye-opening and synaptic refinement (Figure 1c). We found that GLT1 mRNA was developmentally regulated (one-way ANOVA, $F(6,18) = 86.7$, $p = 2.7 \times 10^{-12}$) and that it remained low until ∼P14, around the time of eye-opening (P28: 1.0 ± 0.01, P0: 0.03 ± 0.01, P7:0.18 ± 0.01, P14: 0.89 ± 0.02, P21: 1.28 ± 0.14, P42: 1.02 ± 0.08, P60: 1.04 ± 0.03). GLT1 transcripts peaked around P21 and remained high through P60, indicating that GLT1 function could be important for experience-dependent binocular refinement that occurs during development between ∼P14-34. Furthermore these findings suggest that GLT1 expression may be regulated by visual experience, and thus have a role in driving activity-dependent plasticity in V1.

3.2 | GLT1 heterozygous mice have normal astrocyte morphology and retinogeniculate axonal segregation

In order to gain a deeper understanding of the role of GLT1 in visual cortex development, we used a germline heterozygous knockout GLT1 mouse model. This mouse line (GLT1 HET) had been previously described as a model for glutamatergic hyperactivity, with GLT1 HET mice displaying several behavioral phenotypes (Kiryk et al., 2008; Tanaka et al., 1997) but had not been widely used to study the

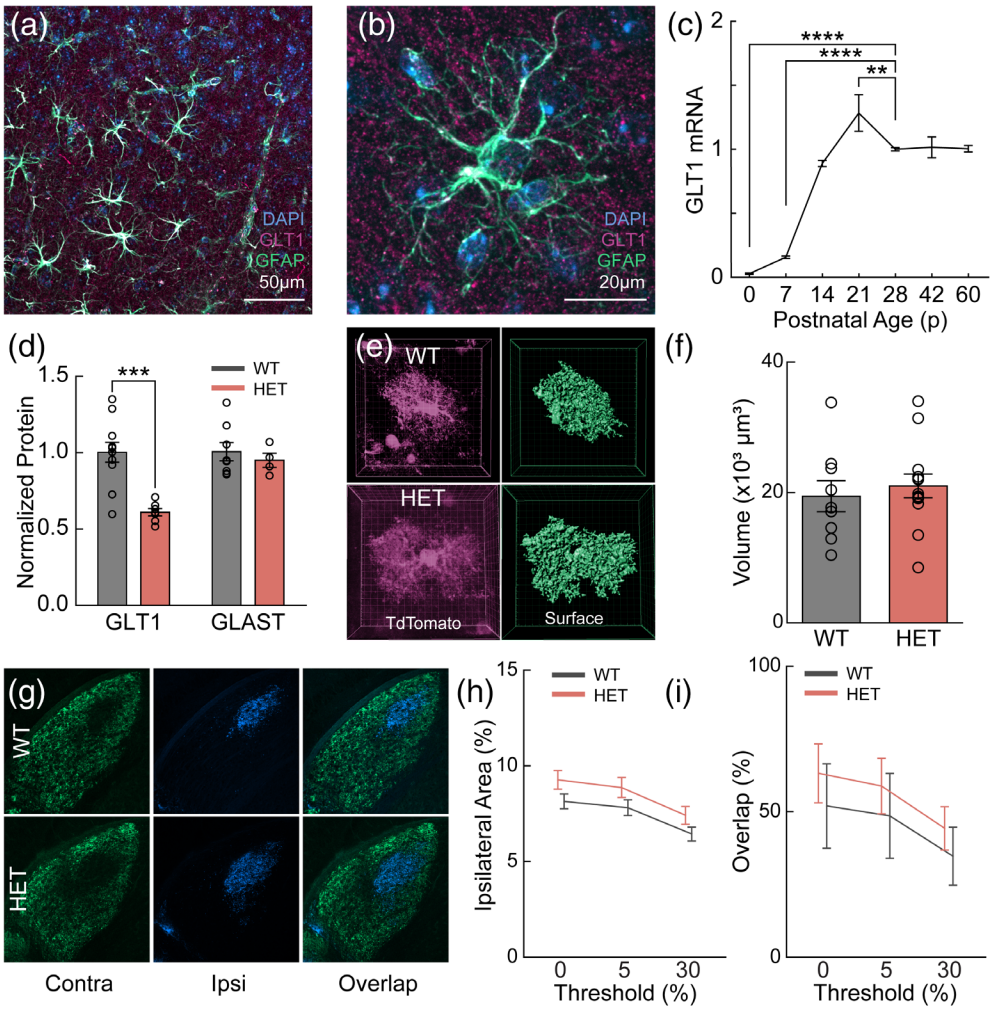

FIGURE 1 GLT1 is upregulated in the developing visual cortex concurrent with visual experience. (a) Immunohistochemical stain of GLT1 (magenta), GFAP (green), and DAPI (blue) at ~P28 in mouse visual cortex. (b) High-magnification image of a single GFAP-labeled astrocyte with surrounding GLT1 expression. (c) Quantification of GLT1-mRNA across developmental time points showing a significant increase from birth and peaking at P21. Levels are normalized to P28 (P0 [n = 4], P7 [n = 4], P14 [n = 3], P21 [n = 3], P28 [n = 4], P42 [n = 3], P60 [n = 4]; one-way ANOVA, $F(6,18) = 86.7$, $p = 2.7 \times 10^{-12}$). (d) Western blot quantification showing that transgenic mice with heterozygous expression of GLT1 (HET) have significantly less GLT1 expression compared to wildtype (WT) littermates (P28, n = WT(11), HET(11); unpaired t-test, $t = 4.64$, $p = 2.7 \times 10^{-4}$), but comparable expression of GLAST (WT [n = 8], HET [n = 4]; unpaired t-test, $t = 0.62$, $p = 0.55$). (e) Example images of GLT1 WT and HET astrocytes labeled using a custom GFAP-tdTomato transgenic mouse line (magenta). Astrocyte volume is reconstruction from imaged z-stacks (green). (f) Quantification of astrocyte volume from 3D reconstructions show no gross volume changes between GLT1 WT and HET animals (WT [n = 3], HET [n = 13]; unpaired t-test, $t = 0.53$, $p = 0.60$). (g) Images of the lateral geniculate nucleus (LGN) after CTB-594 (green) and CTB-488 (blue) injected into the contralateral and ipsilateral eyes respectively. Merged overlays from GLT1 WT and HET mice show normal retinothalamic axon segregation. (h) Quantification of ipsilateral area in GLT1 WT and HETs across several binary thresholds (0, 5, 30%) showing no difference in absolute ipsilateral area (WT [n = 3], HET [n = 6]; two-way ANOVA, genotype effect $F(1,7) = 1.93$, $p = 0.21$). (i) Quantification of contra/ipsi projection overlap showing no difference in contra/ipsi segregation (WT [n = 3]), HET [n = 6]; two-way ANOVA, genotype effect, $F(1,7) = 0.43$, $p = 0.53$). $^{**}p < 0.01$, $^{***}p < 0.005$, $^{****}p < 0.001$ [Color figure can be viewed at wileyonlinelibrary.com]

developing visual cortex. We chose the GLT1 HET line over the GLT1 KO line for several reasons. First, the GLT1 KO line displays several developmental abnormalities (e.g. seizures, brain injury, low body weight; see Kiryk et al., 2008; Tanaka et al., 1997) not present in the GLT1 HET model. Furthermore, the GLT1 KO mice have reduced survival by P21, making them not suited for studies of the visual cortex critical period (which peaks ~P28–30). As expected, GLT1 HET animals expressed significantly reduced levels of GLT1 protein in V1 at P28 (WT: 1.0 ± 0.07, HET: 0.61 ± 0.02; unpaired t-test, $t = 4.64$, $p = 2.7 \times 10^{-4}$; Figure 1d) confirming previous reports (Kiryk et al., 2008). The other major glutamate transporter expressed in the visual cortex of mice, GLAST, was not altered in the GLT1 HETs indicating that there is no compensatory increase in total glutamate transporter protein expression in V1 (WT: 1.0 ± 0.06, HET: 0.95 ± 0.05; unpaired t-test, $t = 0.62$, $p = 0.55$). GLT1 expression has been linked to astrocyte process ramification and synaptic ensheathment (Benediktsson

et al., 2012; Genoud et al., 2006; Zhou & Sutherland, 2004), suggesting that a constitutive decrease in GLT1 expression might alter astrocyte morphology. To examine gross astrocyte morphology in GLT1 HET mice, we crossed them with a GFAP-tDTomato reporter mouse in which astrocytes express tDTomato throughout the cortex. Confocal stacks of tDTomato+ astrocytes were collected from fixed tissue of GLT1 WT and HET mice and 3D-reconstructed using the Imaris software package (Figure 1e). No significant difference was observed in astrocyte volume between GLT1 WT and HET animals (WT: $19.4 \times 10^3 \pm 2.4 \times 10^3$, HET: $21.0 \times 10^3 \pm 1.8 \times 10^3$; unpaired *t*-test, $t = 0.53$, $p = 0.60$) showing that ~40% reduction in GLT1 expression does not significantly alter gross astrocyte cytosolic volume (Figure 1f). As a prelude to examining ocular dominance plasticity in V1, we also investigated whether GLT1 HET mice showed deficits in the activity-dependent segregation of retinogeniculate axons in the lateral geniculate nucleus (LGN). Cholera toxin subunit B conjugated to two distinct fluorophores were individually injected into the contralateral and ipsilateral eyes labeling the eye-specific projections to the LGN (Figure 1g). We found no significant difference between either the ipsilateral axonal area normalized to the contralateral axonal area (two-way ANOVA, genotype effect, $F(1,7) = 1.93$, $p = 0.21$; Figure 1h) nor the overlap between the contralateral and ipsilateral axonal areas (two-way ANOVA, genotype effect, $F(1,7) = 0.43$, $p = 0.53$; Figure 1i). These results demonstrate that GLT1 HET mice have reduced GLT1 expression in V1 at P28, but do not exhibit gross morphological deficits in astrocytes or axonal segregation of retinogeniculate projections in the LGN, and hence in the anatomical extent of retinal drive to visual cortex.

3.3 | Visual cortex neurons in GLT1 HET mice have abnormally high ipsilateral responses and poor binocular matching of preferred orientation

We next examined the functional consequences of GLT1 reduction on experience-dependent refinement of binocular inputs to the visual cortex. During normal development, binocular cells in the contralateral cortex that respond to visual input from both the contralateral and ipsilateral eyes (Figure 2a) refine their activity to (a) scale responses from the two eyes, and (b) match their preferred activity from both eyes to similarly specific orientations (Gu & Cang, 2016; Hooks & Chen, 2020). To test whether GLT1 HET mice have alterations in the magnitude and refinement of binocular inputs, we examined several measures of neuronal responses to visual gratings stimulating either the contralateral or ipsilateral eye (Figure 2a). We used two-photon microscopy in awake, head-fixed mice to image neuronal responses in V1 of GLT1 WT or HET mice at ~P28. We stimulated the contralateral and ipsilateral eyes independently with gratings of different orientations and examined the calcium responses (Figure 2b). We then calculated independent tuning curves to grating orientation for both contralateral and ipsilateral input. We qualitatively observed striking differences between GLT1 WT and GLT1 HET mice. Neuronal responses to gratings in GLT1 WT mice had similar tuning curves to gratings presented to either the contralateral or ipsilateral eye, showing the expected matching of preferred orientation between the two eyes. In addition, responses to contralateral input was higher than ipsilateral input as expected for a normal contralateral bias in responses (Figure 2b, top). Conversely, neuronal responses to gratings in GLT1 HET mice had qualitatively mismatched tuning between contralateral and ipsilateral eye input, and abnormally high ipsilateral response magnitudes (Figure 2b, bottom). To quantify the neuronal responses between genotypes, we first examined whether there was a difference in the magnitude of the response to the preferred orientation (Figure 2c) regardless of the specific preferred orientation angle. We found that, as expected, the average response to preferred orientation of binocular neurons was significantly higher to contralateral inputs relative to ipsilateral inputs in GLT1 WT mice (WT-C/I: 0.30 ± 0.02/0.22 ± 0.01, HET-C/I: 0.32 ± 0.03/0.33 ± 0.03; one-way ANOVA, $F(3,674) = 6.44$, $p = 2.7 \times 10^{-4}$), demonstrating the contralateral bias (Holm–Sidak, $t = 3.39$, $p = 4.0 \times 10^{-3}$). However, GLT1 HET neurons displayed comparable response magnitudes to contralateral and ipsilateral input (Holm–Sidak, $t = 0.25$, $p = 0.85$). These response magnitudes were significantly higher than ipsilateral response magnitudes (Holm–Sidak, $t = 3.42$, $p = 3.9 \times 10^{-3}$) and comparable to contralateral response magnitudes in GLT1 WT mice (Holm–Sidak, $t = 0.80$, $p = 0.81$; Figure 2c). To directly compare the ratio of responses to contralateral and ipsilateral stimuli, we calculated the ocular dominance index (ODI) for each neuron across genotypes (see methods for ODI calculation, Figure 2d). We found that neurons in GLT1 HET mice had a significantly decreased ODI indicating a decrease in the normal contralateral bias (WT: 0.14 ± 0.02, HET: 0.01 ± 0.04; unpaired *t*-test, $t = 3.15$, $p = 1.8 \times 10^{-3}$). Though there appeared to be increased ODI variance between GLT1 WT and HET mice, there was only borderline significance ($F(1.372)$, $p = 0.053$).

We next asked whether the orientation specificity to tuned responses was different between GLT1 WT and HET mice. We calculated the global OSI according to previous reports (Banerjee et al., 2016) for each neuron and for contralateral and ipsilateral visual stimulation (Figure 2e). We found that in GLT1 WT mice, the OSI was comparable for both contralateral and ipsilateral eye responses (WT-C: 0.31 ± 0.01, WT-I: 0.30 ± 0.01; one-way ANOVA, $F(3,674) = 6.12$, $p = 4.1 \times 10^{-4}$; Holm–Sidak, $t = 0.78$, $p = 0.65$). However, in GLT1 HET mice, ipsilateral responses had a significantly lower OSI compared to both contralateral (HET-I: 0.23 ± 0.01, WT-C: 0.31 ± 0.01; Holm–Sidak, $t = 4.16$, $p = 1.1 \times 10^{-4}$) and ipsilateral responses (HET-I: 0.23 ± 0.01, WT-I: 0.30 ± 0.01; Holm–Sidak, $t = 3.56$, $p = 2.0 \times 10^{-3}$) in WT mice, and a trend towards decreased OSI relative to contralateral responses in GLT1 HET mice (HET-C: 0.28 ± 0.02, HET-I: 0.23 ± 0.01; Holm–Sidak, $t = 2.30$, $p = 0.08$). These results demonstrate that ipsilateral responses in GLT1 HET mice are less specific to orientation tuning than WT mice. Finally, to quantify the degree to which contralateral and ipsilateral peak responses were tuned to the same orientation, indicating binocular matching, we calculated the difference in preferred orientation angle between peak contralateral and ipsilateral input (ΔPO; Figure 2f). We found that GLT1 HET neurons had significantly higher difference in preferred orientation angle compared to GLT1 WT neurons (WT:

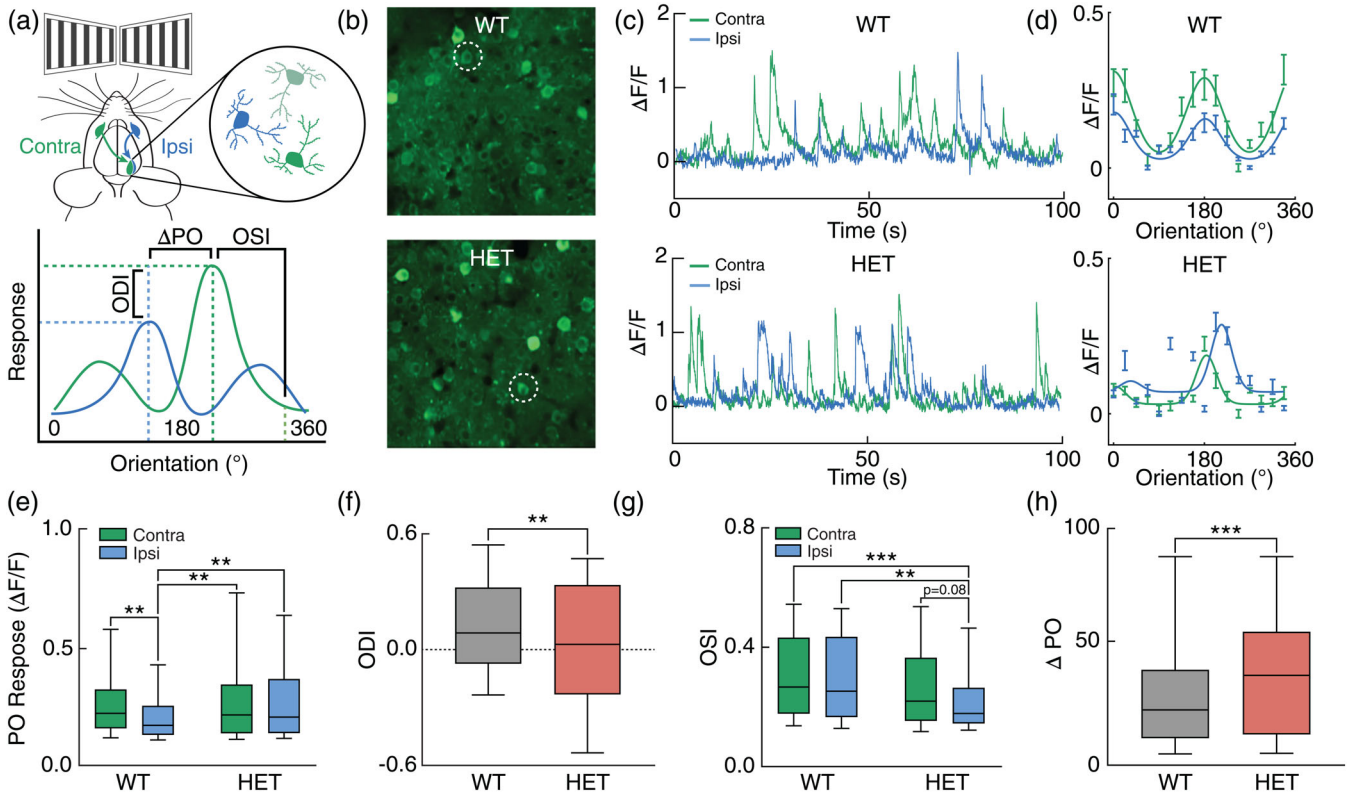

FIGURE 2 GLT1 HET mice have higher ipsilateral eye responses, lower contralateral eye bias and disrupted experience-dependent binocular matching of orientation-selective responses. (a) Top: Visual gratings were separately presented to the contra (green) and ipsi (blue) eyes in P28 mice and neuronal responses recorded. Bottom: schematic of measures. Ocular dominance index (ODI) was calculated as $(max^{Contra} - max^{Ipsi})/max^{Contra} + max^{Ipsi}$. Orientation Selectivity Index (OSI) is calculated as before (Banerjee et al., 2016). Difference in preferred orientation (ΔPO) is calculated as the difference between preferred orientations of the max contralateral and ipsilateral responses. (b) Example field of views in binocular visual cortex from GLT1 WT (top) and GLT1 HET (bottom) mice. Neuronal activity was quantified using the GCaMP6f calcium indicator (green). (c) Example calcium traces from cells circled in B showing responses to grating presentations to either the contralateral (blue) or ipsilateral (green) eye. Note grating presentation order was pseudorandom and therefore temporal sequences are different for each eye. (d) Two example neuronal tuning curves with contra (green) and ipsi (blue) stimulation. Lines represent best double-gaussian fits (see Section 2). (e) Average response to PO of contra and ipsi stimulation in GLT1 WT and HET mice. WT mice had significantly higher contra eye responses while HET mice have approximately equal responses to each eye (n = 4–6 animals, 23–52 cells per animal, two-way ANOVA, genotype $F(1,674) = 7.72$, $p = 0.0056$, interaction $F(1,674) = 4.243$, $p = 0.040$). (f) Quantification of ocular dominance index showing that GLT1 HET mice have significantly decreased ODI (n = 4–6 animals, 23–52 cells per animal, t-test, $p = 0.0018$). (g) Quantification of OSI showing that GLT1 HET mice have a significantly decreased OSI of ipsilateral responses compared to both contra and ipsi responses in GLT1 WT animals (n = 4–6 animals, 23–52 cells per animal, two-way ANOVA, genotype $F(1,674) = 12.46$, $p = 4.5 \times 10^{-4}$). (h) Quantification of ΔPO showing an increased difference in the preferred orientations between contralateral and ipsilateral inputs to neurons in GLT1 HET animals (n = 4–6 animals, 23–52 cells per animal, t-test, $p = 1.0 \times 10^{-4}$). *$p < 0.05$, **$p < 0.01$, ***$p < 0.005$. Box–Whisker plots represent median, 10th,25th, 75th, and 90th percentiles [Color figure can be viewed at wileyonlinelibrary.com]

24.3 ± 1.37, HET: 35.1 ± 2.71; unpaired t-test, $t = 3.93$, $p = 1.0 \times 10^{-4}$). Together, these results reveal that in GLT1 HET mice, ipsilateral eye responses are abnormally high leading to reduced ODI, decreased OSI, and an increased in ΔPO, altogether signifying increased ipsilateral drive and disrupted binocular matching.

3.4 | GLT1 HET mice have abnormal spine density and synapse function

Given the observed changes in response magnitude and specificity in GLT1 HET mice, we next asked whether changes in structural features of layer 2/3 V1 neurons and in synaptic transmission might explain our neurophysiological results. We reasoned that if eye-specific responses and binocular matching were disrupted by excess extracellular glutamate, synapses that were normally pruned in an activity-dependent manner might be abnormally retained. To examine this possibility, we crossed the GLT1 HET mice with a Thy1-GFPm mouse line (Feng et al., 2000) that expresses GFP in a subset of neurons across the brain. We chose this line because labeling of layer 2/3 neurons in the visual cortex is relatively sparse, which allowed us to examine synaptic spine density on clearly labeled dendrites (Figure 3a). We focused histological and electrophysiological analyses on layer 2/3 neurons to compare results with the in vivo physiology (Figure 2). We collected brain slices from ~P28 GLT1 WT and HET mice and analyzed the dendritic spine density on basal dendrites of

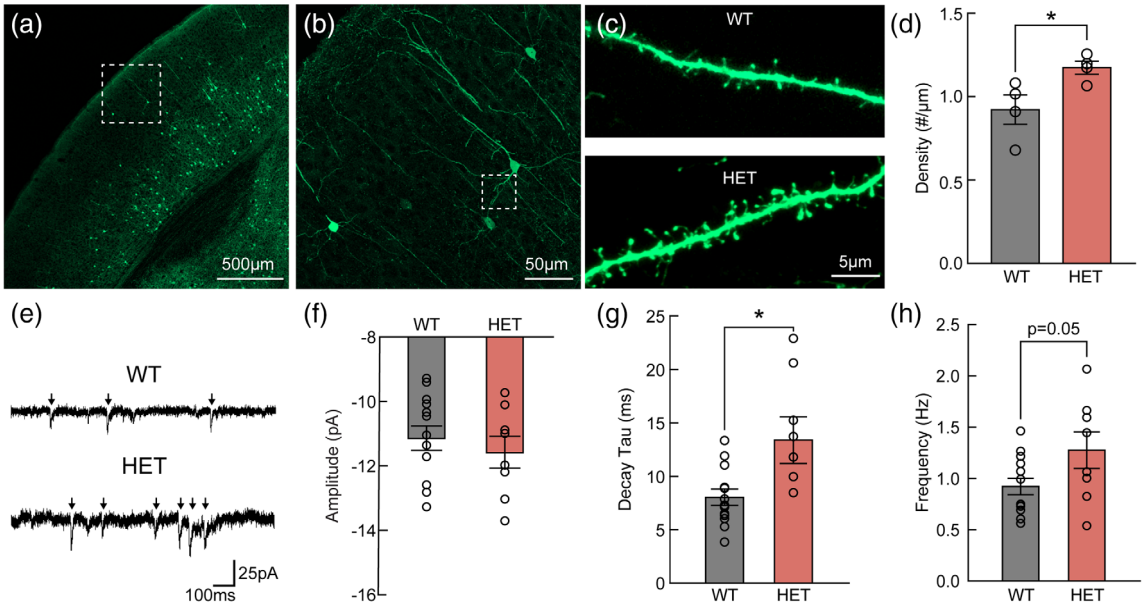

FIGURE 3 GLT1 HET mice have abnormal spine density and synapse function. (a) Low-magnification image of neurons in visual cortex of GFP-M transgenic mice. (b) higher-magnification image of layer 2/3 neurons (dotted box in A). (c) Images of basal dendrites of layer 2/3 neurons in GLT1 WT (top) and HET (bottom) mice. WT example is from dotted box in B. (d) GLT1 HET mice have increased spine density on basal dendrites of layer 2/3 neurons in visual cortex (n = 4 animals, 5 slices, 10 dendrites per animal, t-test, p = 0.041). (e) Example traces of miniature excitatory post-synaptic currents (mEPSCs, arrows) from voltage-clamped layer 2/3 neurons in the visual cortex of GLT1 WT and HET. (f) Quantification of mEPSC amplitude showing no difference in magnitude of mEPSCs (n = 8–13 cells, t-test, p = 0.49). (g) GLT1 HET mEPSCs have significantly higher decay time (n = 8–13 cells, t-test, p = 0.013). (h) GLT1 HET mEPSCs trend towards increased $^*p < 0.05$ [Color figure can be viewed at wileyonlinelibrary.com]

layer 2/3 excitatory neurons (Figure 3b,c). We found a significant increase in dendritic spine density (WT [n = 4]: 0.92 ± 0.09, HET [n = 4]: 1.18 ± 0.04; unpaired t-test, t = 2.60, p = 0.04) (Figure 3d). We next asked whether the increased dendritic spine density resulted in an increase in functional synapses as measured by miniature excitatory post-synaptic currents (mEPSCs) in V1 neurons in slices from GLT1 WT and HET mice at ∼P28. Layer 2/3 neurons were whole-cell patched and mEPSCs measured (Figure 3e). We found no difference in the amplitude of mEPSCs between GLT1 WT and HET neurons (WT [n = 13 cells]: −11.1 ± 0.38, HET [n = 8 cells]: −11.6 ± 0.49; unpaired t-test, t = 0.70, p = 0.49; Figure 3f). However, as would be expected from decreased glutamate uptake, we did observe a significant increase in the decay time of events (WT [n = 13 cells]: 8.04 ± 0.76, HET [n = 8 cells]: 13.39 ± 2.19, unpaired t-test, t = 2.75, p = 0.013; Figure 3g). In addition, there was a trend toward increased mEPSC frequency suggesting that GLT1 HET mice had increased excitatory input (WT [n = 13 cells]: 0.92 ± 0.08, HET [n = 8 cells]: 1.28 ± 0.18; unpaired t-test, t = 2.07, p = 0.05; Figure 3h).

3.5 | GLT1 HET mice have disrupted ocular dominance plasticity

Our observations suggest that experience-dependent synaptic refinement underlying ipsilateral response amplitude and binocular orientation matching is altered in GLT1 HET mice. Therefore, we asked whether experience-dependent synaptic plasticity is broadly altered in GLT1 HET mice. To address this question, we used the classic ocular dominance plasticity (ODP) model of synaptic plasticity in which one eye is deprived of visual input for 4–7 days during the critical period for ODP (∼P21–P35 in mice). This deprivation drives a broad network shift in the contralateral visual cortex of preferred responsiveness from the deprived eye (typically the contralateral eye) toward the eye that remained open (typically the ipsilateral eye) (Hooks & Chen, 2020). Previous work has demonstrated that 7 days of monocular deprivation (MD) leads first to a decrease in responsiveness to the closed eye in the first 3–4 days followed by potentiation of responsiveness to the open eye (Smith, Heynen, & Bear, 2009). The degree to which this shift occurs indicates the degree to which cortical circuits are able to functionally and structurally rearrange in response to changes in sensory input. To assess ODP in GLT1 WT and HET mice, we used intrinsic signal optical imaging, which has been used to characterize large-scale neuronal response to visual stimuli across V1 (Cang, Kalatsky, Lowel, & Stryker, 2005). GLT1 WT and HET mice at ∼P28 were either not deprived (ND), or monocularly deprived for 4 days (4dMD) or 7 days (7dMD). Contralateral and ipsilateral eyes were then stimulated individually, and V1 contralateral to the deprived eye imaged. A drifting bar was used to evoke a retinotopic map of activity and the binocular region was selected to evaluate the amplitude of response elicited by contralateral and ipsilateral eye stimulation (Figure 4a).

We calculated the ODI of imaged pixels to evaluate relative responses to contralateral and ipsilateral eye stimulation. We first

recapitulated normal ODP in ND GLT1 WT mice as evidenced by a strong contralateral bias (ODI > 0.3, Figure 4b). Following 4dMD, GLT1 WT mice displayed a normal ocular dominance shift with significant reduction in ODI (WT-ND [n = 4]: 0.35 ± 0.04, WT-4dMD [n = 4]: 0.05 ± 0.02; Holm–Sidak, $t(18) = 4.83$, $p = 2.7 \times 10^{-4}$). Following 7dMD we observed a further significant shift in ODI resulting in a slight ipsilateral bias (WT-ND [n = 4]: 0.35 ± 0.04, WT-7dMD [n = 4]: −0.07 ± 0.01; Holm–Sidak, $t(18) = 6.83$, $p = 6.5 \times 10^{-6}$). Next, we repeated the imaging in GLT1 HET mice and found that unlike WT controls, ND HET animals showed a significantly reduced ODI consistent with our single-cell calcium recordings (see Figure 2d). Following 4dMD, GLT1 HET mice showed a strong ocular dominance shift resulting in a pronounced ipsilateral bias, and demonstrating that ODP was intact (HET-ND [n = 4]: 0.02 ± 0.02, HET-4dMD [n = 4]: −0.17 ± 0.02; Holm–Sidak, $t(18) = 3.03$, $p = 0.02$). Surprisingly, after 7dMD GLT1 HET mice had a significant ocular dominance shift back towards contralateral responsiveness, indicating plasticity opposite to the direction of experience-dependent potentiation (HET-4dMD [n = 4]: −0.17 ± 0.02, HET-7dMD [n = 4]: 0.002 ± 0.02; Holm–Sidak, $t(18) = 2.76$, $p = 0.03$). In order to explain these counterintuitive results, we examined the individual response amplitudes to each eye across 4dMD and 7dMD. In GLT1 WT mice, we observed a significant increase in responsiveness to the ipsilateral eye consistent with previous work (Figure 4c, WT-ND-I [n = 4]: 3.01 ± 0.15, WT-4dMD-I [n = 4]: 4.4 ± 0.24; Holm–Sidak, $t(36) = 2.48$, $p = 0.04$; WT-ND-I [n = 4]: 3.01 ± 0.15, WT-7dMD-I [n = 4]: 5.13 ± 0.11; Holm–Sidak, $t(36) = 3.74$, $p = 1.9 \times 10^{-3}$) (Sato & Stryker, 2008). However, in GLT1 HET mice, we observed an overall decrease in contralateral and ipsilateral responsiveness at both 4dMD and 7dMD with the contralateral response decreasing in amplitude at 4dMD (Figure 4c, HET-ND-C (n = 4): 4.75 ± 0.23, HET-4dMD-C: 3.24 ± 0.17; Holm–Sidak, $t(36) = 2.63$, $p = 0.02$) and 7dMD (HET-ND-C [n = 4]: 4.75 ± 0.23, HET-7dMD-C: 2.55 ± 0.28; Holm–Sidak, $t(36) = 3.81$, $p = 1.6 \times 10^{-3}$), and ipsilateral response at 7dMD (HET-ND-I [n = 4]: 4.65 ± 0.20, HET-7dMD-I: 3.14 ± 0.11; Holm–Sidak, $t(36) = 2.60$, $p = 0.04$). These results suggest that GLT1 HET mice show an abnormal decrease in ipsilateral responsiveness with MD. Therefore, the increase in ODI from 4dMD to 7dMD in GLT1 HETs reflects a predominating decrease in ipsilateral responses rather than an increase in contralateral responses.

3.6 | GLT1 expression in GLT1 HET mice is modulated by monocular deprivation

Previous work has demonstrated that GLT1 protein expression and translocation are influenced by changes in neuronal activity (Benediktsson et al., 2012; Murphy-Royal et al., 2015). Although GLT1 HET mice have ∼40% reduction in protein at ∼P28 in the absence of MD, it is possible that MD affects GLT1 expression in the remaining copy of the GLT1 gene. To assess this possibility, we measured GLT1 mRNA levels in GLT1 WT and HET mice either in ND or 4dMD and 7dMD conditions (Figure 5a). In ND mice, we observed the expected decrease in GLT1 HET mice relative to WT controls (WT-ND [n = 2]: 1.00 ± 0.02, HET-ND [n = 3]: 0.60 ± 0.02; Holm–Sidak, $t(9) = 2.95$, $p = 0.02$). Interestingly, in GLT1 HET mice, we observed a significant increase in GLT1 mRNA at 4dMD (HET-ND [n = 3]: 0.60 ± 0.04, HET-4dMD [n = 3]: 1.16 ± 0.04; Holm–Sidak, t

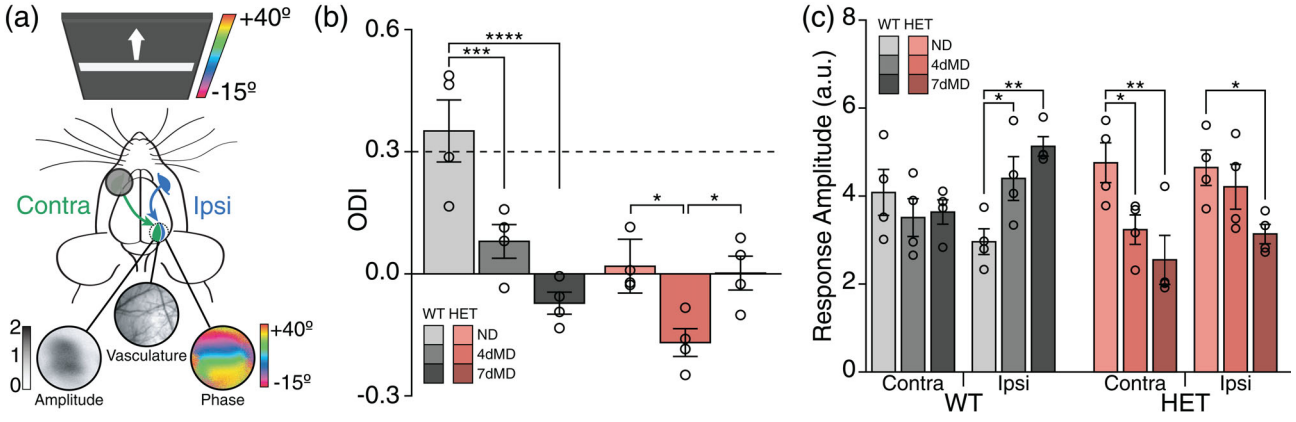

FIGURE 4 GLT1 HET mice have disrupted ocular dominance plasticity. (a) Schematic of experimental setup for intrinsic signal optical imaging. Drifting bars are presented to each eye individually and phase maps are generated by the retinotopic activity in visual cortex. Averaged responses of multiple sweeps yield an amplitude map. Ocular dominance index (ODI) is calculated as the contralateral response − ipsilateral response/contralateral + ipsilateral responses. (b) ODI for GLT1 WT (grays) and GLT1 HET (reds) mice that were either nondeprived (ND), or had the contralateral eye monocularly deprived for 4 days (4dMD) or 7 days (7dMD). GLT1 WT mice display a typical contralateral bias in ND conditions. After 4dMD and 7dMD the ODI significantly decreases demonstrating intact ocular dominance plasticity. GLT1 HET mice display an abnormal lack of contralateral ODI bias under ND conditions, a significant decrease in ODI at 4dMD, and a return to no bias at 7dMD (n = 4 animals per group, two-way ANOVA, Holm–Sidak post-hoc comparisons). (c) Comparison of eye-specific amplitudes for GLT1 WT and HET mice. ND GLT1 HET mice have approximately equal responses to contralateral and ipsilateral inputs. After 4dMD, GLT1 HET mice have a significant decrease in contralateral responses and at 7dMD, significant decrease in both contralateral and ipsilateral responses (n = 4 animals per group, two-way ANOVA, Holm–Sidak post-hoc comparisons). *p < 0.05, **p < 0.01, ***p < 0.005 [Color figure can be viewed at wileyonlinelibrary.com]

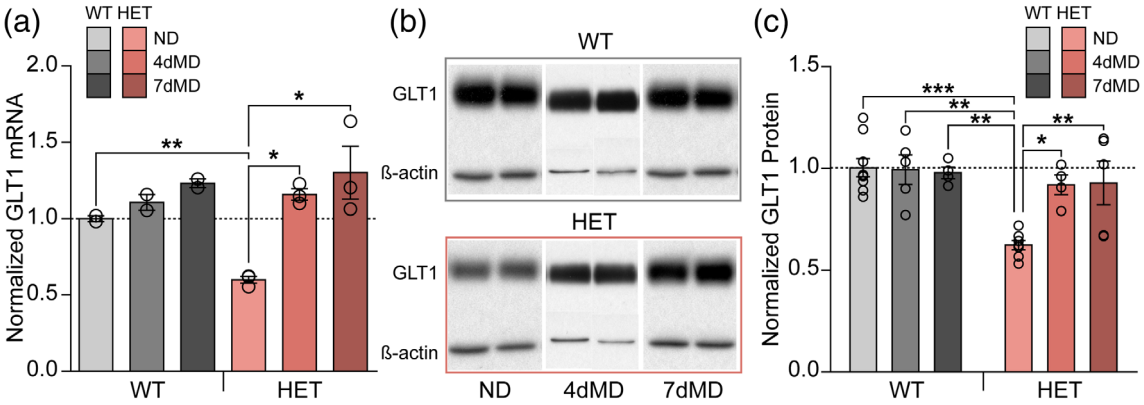

FIGURE 5 GLT1 HET mice have upregulation of GLT1 expression during monocular deprivation. (a) Quantification of GLT1 mRNA in WT (grays) and HET (reds) mice in ND, 4dMD, and 7dMD conditions. GLT1 HET mice have significantly less GLT1 mRNA in ND conditions, but no difference at 4dMD and 7dMD compared to WT mice (n = 2–3 animals per group, two-way ANOVA, Holm–Sidak post-hoc comparisons). (b) Example western blots for GLT1 protein in WT (top) and HET (bottom) mice in ND, 4dMD, and 7dMD conditions. (c) Quantification of western blots showing significantly less GLT1 protein in HET mice in ND, but no difference in 4dMD and 7dMD compared to WT littermates (n = 4–9 animals per group, two-way ANOVA, Holm–Sidak post-hoc comparisons). *p < 0.05, **p < 0.01, ***p < 0.005 [Color figure can be viewed at wileyonlinelibrary.com]

(9) = 4.60, $p = 2.6 \times 10^{-3}$) and 7dMD (HET-ND [n = 3]: 0.60 ± 0.04, HET-7dMD [n = 3]: 1.30 ± 0.17; Holm–Sidak, t(9) = 4.60, $p = 2.6 \times 10^{-3}$), suggesting that MD increases GLT1 expression in a haplosufficient manner. To determine whether increases in GLT1 mRNA lead to increased GLT1 protein, we performed western blot analysis of GLT1 protein in GLT1 WT and HET mice at either ND, 4dMD, or 7dMD (Figure 5b). We reproduced our previous data showing an ~40% reduction in GLT1 protein in ND GLT1 HET mice compared to WT controls (WT-ND [n = 9]: 1.0 ± 0.02, HET-ND [n = 7]: 0.61 ± 0.01; Holm–Sidak, t(28) = 5.42, $p = 1.3 \times 10^{-4}$). However, GLT1 HET mice had an increase in GLT1 protein following 4dMD (HET-ND [n = 7]: 0.61 ± 0.01, HET-4dMD [n = 4]: 0.91 ± 0.02; Holm–Sidak, t(28) = 3.39, p = 0.02) and 7dMD (HET-ND [n = 7]: 0.61 ± 0.01, HET-7dMD [n = 4]: 0.92 ± 0.05; Holm–Sidak, t(28) = 3.74, p = 0.01). The fact that GLT1 WT mice did not have a significant increase in GLT1 protein with MD indicates that increased GLT1 in HET mice with MD is a haploinsufficient phenotype. Importantly, these data reveal that GLT1 HET mice specifically have an increase in GLT1 protein to WT levels in response to MD, which may underlie their abnormal ocular dominance plasticity after MD.

4 | DISCUSSION

In summary (Figure 6), we confirmed that astrocytes in the visual cortex express high levels of GLT1 protein in the visual cortex at ~P28. GLT1 transcription increased in the visual cortex around eye-opening and the onset of experience-dependent synaptic refinement, peaked around P21 and remained high into adulthood. We confirmed that GLT1 HET mice have ~40% reduction in GLT1 protein at P28, the peak of the critical period for visual cortex plasticity. GLT1 HET mice seemed to have normal gross astrocyte morphology and retinal axonal segregation in the LGN. Single-cell visual responses in the binocular V1 at P28 revealed that GLT1 HET mice have abnormally high ipsilateral eye responses, concomitant with increased discrepancy of preferred orientation angle between contralateral and ipsilateral responses, decreased ipsilateral OSI, and decreased ODI. Histological characterization of GLT1 HET mice demonstrated increased dendritic spine density in layer 2/3 pyramidal neurons, and electrophysiological recordings revealed increased frequency and decay time constants for layer 2/3 mEPSCs. Finally, GLT1 HET mice showed a robust ocular dominance shift at 4dMD consistent with reduction of deprived, contralateral eye responses. However, they showed a paradoxical decrease in nondeprived, ipsilateral eye responses at 7dMD, resulting in an atypical positive shift in ODI. This reduction of ipsilateral eye responses followed an increase in GLT1 protein expression after MD. These findings reveal two surprising features of activity-dependent development in the mouse primary visual cortex that are influenced by astrocyte glutamate transporters: increased ipsilateral eye response magnitude during typical visual experience concurrent with reduced GLT1 expression, and an anomalous effect of MD on eye-specific responses with a reduction in ipsilateral eye responses, concurrent with increased GLT1 expression.

Previous work has demonstrated that glia cells are critical players in both early synaptic refinement and adolescent plasticity including microglial roles in retinothalamic axonal pruning and synaptic remodeling in ocular dominance plasticity (Schafer et al., 2012; Sipe et al., 2016; Stowell et al., 2019). With regards to astrocytic roles in visual cortex development, evidence suggests that astrocytes are able to drive the plasticity of neuronal circuits (Foxworthy & Medina, 2015; Muller & Best, 1989; Singh et al., 2016). Though astrocytes are known to release neuroactive factors to promote synapse formation, our results show that glutamate uptake via GLT1 is another crucial function of astrocytes in synaptic development and plasticity of the visual cortex.

Although we quantified gross astrocyte volume and found no significant differences between GLT1 WT and HET mice, we did not

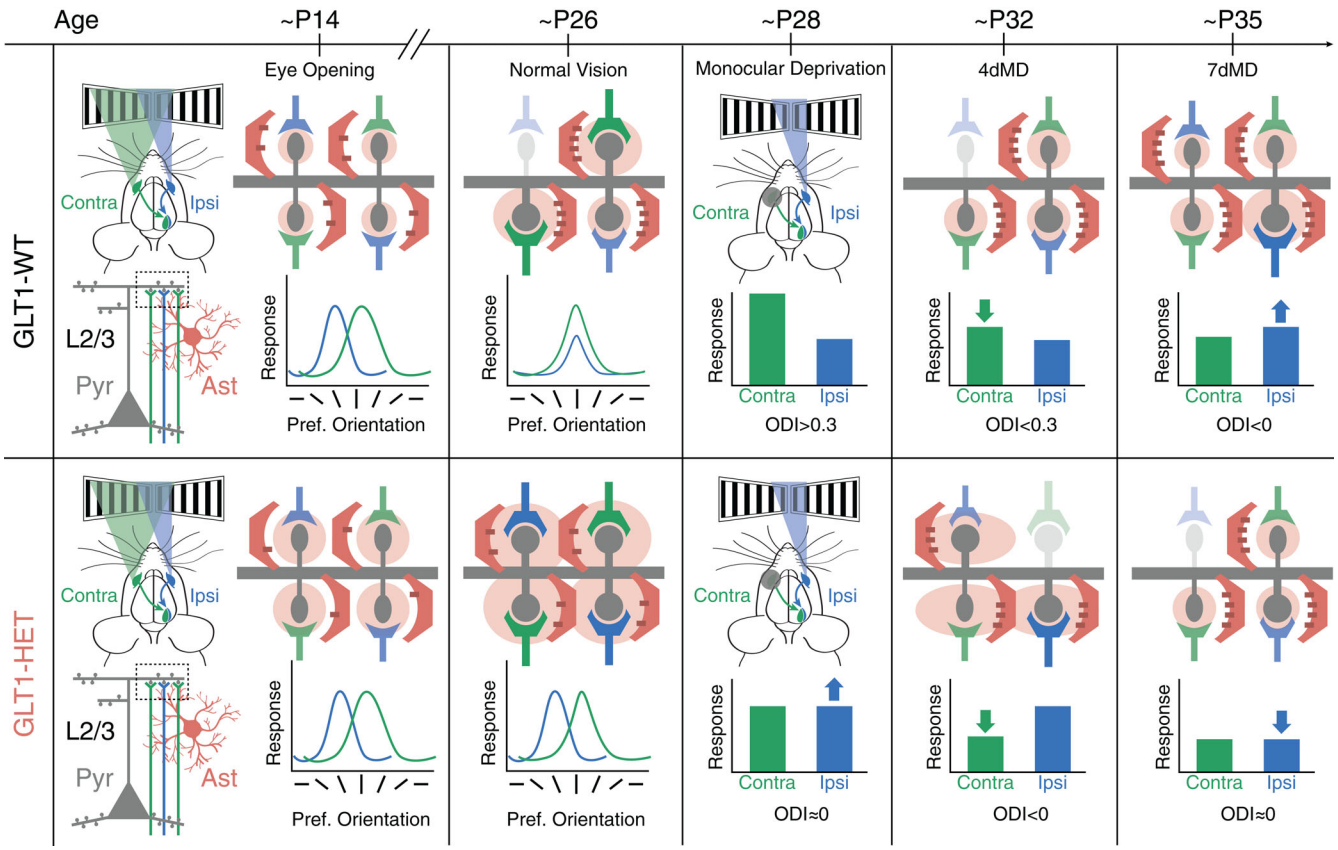

FIGURE 6 Summary and model of experimental results. (a) Schematic showing the contralateral (contra, green) and ipsilateral (ipsi, blue) inputs to binocular visual cortex synapsing onto layer 2/3 pyramidal cells (L2/3, Pyr, gray). Astrocytes (Ast, orange) have fine processes that surround excitatory synapses. Dashed box is magnified below, with details. (b) At eye-opening, GLT1 WT and HET animals have similar astrocyte volume and LGN refinement. With visual experience, GLT1-WT animals undergo activity-dependent plasticity resulting in decreased spine density, binocular matching of preferred orientation, and a contralaterally biased ocular dominance. GLT1-HET animals have comparatively decreased GLT1 protein resulting in increased dendritic spines, increased ipsi responses, reduced contra bias and orientation tuning, and decreased binocular matching of orientation preference. Following 4 days of MD in GLT1-WT mice, contralateral responses decrease and after 7 days of MD, ipsilateral responses increase. In GLT1-HET animals, after 4 days of MD contralateral responses decrease resulting in a negative ODI. However, after 7 days of MD, increased GLT1 expression also decreases ipsilateral inputs resulting in no ocular dominance bias. These results are reasonably explained by a selective influence of GLT1 on ipsilateral inputs and responses during development [Color figure can be viewed at wileyonlinelibrary.com]

explore the possibility of altered fine astrocyte process morphology surrounding synaptic clefts where GLT1 is likely to prevent excess glutamate spillover and sharpen the temporal profile of postsynaptic potentials (Allen & Eroglu, 2017; Huang et al., 2004; Huang & Bergles, 2004). Previous work has indicated that synaptic activity and maturation is associated with astrocyte coverage and GLT1 translocation (Benediktsson et al., 2012; Felix, Stephan, & Rose, 2020; Murphy-Royal et al., 2015; Zhou & Sutherland, 2004). Interestingly, a small proportion of GLT1 is expressed in neurons and seems to correlate with synaptic maturity (Danbolt, Furness, & Zhou, 2016; Herde et al., 2020; Petr et al., 2015). These results suggest that perhaps astrocyte GLT1 expression and synaptic localization are particularly important for synaptic refinement, which could explain increased spine density and ectopic ipsilateral visual responses observed in the GLT1 HET mice. Therefore, future work will be needed to clarify the mechanisms relating developmental synaptic refinement to particular subsets of synapses, the role of astrocytes and GLT1, and the microstructure of the tripartite synapse.

The unexpected result that GLT1 reduction leads to abnormally high ipsilateral responses, broader tuning, and mismatched binocular orientation preference can be reasonably explained by: (a) excess glutamate availability at synapses, increased glutamate spillover, and aberrant synaptic pruning; and (b) spatiotemporal control of glutamate at excitatory synapses on features of visual cortex development, including binocular response magnitude and orientation matching. It is possible that distinct cellular mechanisms differentially regulate contralateral and ipsilateral responses and plasticity. For example, it has recently been shown that Homer1a specifically and actively establishes the contralateral bias intrinsic to binocular-responsive cells (Chokshi, Druciak, Worley, & Lee, 2019). Our work indicates that ipsilateral response depression may be more susceptible to changes in GLT1-mediated glutamate uptake. Further work will be needed to

explore whether GLT1 expression is differentially regulated at eye-specific synapses.

Perhaps the most surprising result of our study is the paradoxical observation that MD leads to reduction of nondeprived ipsilateral eye responses following 7dMD. This effect is overlaid on an increased magnitude of ipsilateral eye responses in ND, or pre-MD, conditions. It may be reasonably explained by a homeostatic increase in GLT1 levels in HET animals after MD, and a subsequent specific effect on ipsilateral eye responses that works to re-establish contralateral bias. The fact that ipsilateral deprived eye responses decrease rather than show their usual potentiation after 7dMD supports the idea that GLT1 upregulation is potently coupled to altered synaptic drive, and surprisingly, serves specifically to reduce ipsilateral eye drive relative to contralateral eye drive. It is possible that the switch from genetically driven synaptic organization to experience-dependent synapse refinement marks the upregulation of GLT1 protein in the visual cortex. These results corroborate previous experiments in somatosensory cortex (Takasaki et al., 2008) in providing clear evidence for the crucial role of GLT1 in early brain development and plasticity.

ACKNOWLEDGMENTS

We thank Taylor Johns, Vincent Pham, Liadan Maire, Stephanie Chou, and Travis Emery for technical assistance, and Kohichi Tanaka and Jeffrey Rothstein for the GLT1 HET mice. Supported by 1F32EY028028 to GOS, 1F32EY022264 to JP, and NIH grants R01EY028219 and R01DA049005 to MS.

CONFLICT OF INTEREST

The authors have no conflicts of interest to declare.

DATA AVAILABILITY STATEMENT

The data that support the findings of this study are available from the corresponding author upon reasonable request. Source data are provided with this paper.

ORCID

Grayson O. Sipe https://orcid.org/0000-0002-1553-7068
Rajeev V. Rikhye https://orcid.org/0000-0003-2011-2897
Mriganka Sur https://orcid.org/0000-0003-2442-5671

REFERENCES

Aida, T., Ito, Y., Takahashi, Y. K., & Tanaka, K. (2012). Overstimulation of NMDA receptors impairs early brain development in vivo. *PLoS One*, *7*, e36853.

Aida, T., Yoshida, J., Nomura, M., Tanimura, A., Iino, Y., Soma, M., … Tanaka, K. (2015). Astroglial glutamate transporter deficiency increases synaptic excitability and leads to pathological repetitive behaviors in mice. *Neuropsychopharmacology*, *40*, 1569–1579.

Allen, N. J., & Eroglu, C. (2017). Cell biology of astrocyte-synapse interactions. *Neuron*, *96*, 697–708.

Antonini, A., Fagiolini, M., & Stryker, M. P. (1999). Anatomical correlates of functional plasticity in mouse visual cortex. *The Journal of Neuroscience*, *19*, 4388–4406.

Araque, A., Carmignoto, G., Haydon, P. G., Oliet, S. H., Robitaille, R., & Volterra, A. (2014). Gliotransmitters travel in time and space. *Neuron*, *81*, 728–739.

Banerjee, A., Rikhye, R. V., Breton-Provencher, V., Tang, X., Li, C., Li, K., … Sur, M. (2016). Jointly reduced inhibition and excitation underlies circuit-wide changes in cortical processing in Rett syndrome. *Proceedings of the National Academy of Sciences of the United States of America*, *113*, E7287–E7296.

Benediktsson, A. M., Marrs, G. S., Tu, J. C., Worley, P. F., Rothstein, J. D., Bergles, D. E., & Dailey, M. E. (2012). Neuronal activity regulates glutamate transporter dynamics in developing astrocytes. *Glia*, *60*, 175–188.

Bhaumik, B., & Shah, N. P. (2014). Development and matching of binocular orientation preference in mouse V1. *Frontiers in Systems Neuroscience*, *8*, 128.

Campbell, S. L., & Hablitz, J. J. (2004). Glutamate transporters regulate excitability in local networks in rat neocortex. *Neuroscience*, *127*, 625–635.

Cang, J., Kalatsky, V. A., Lowel, S., & Stryker, M. P. (2005). Optical imaging of the intrinsic signal as a measure of cortical plasticity in the mouse. *Visual Neuroscience*, *22*, 685–691.

Chokshi, V., Druciak, B., Worley, P. F., & Lee, H. K. (2019). Homer1a is required for establishment of contralateral bias and maintenance of ocular dominance in mouse visual cortex. *The Journal of Neuroscience*, *39*, 3897–3905.

Cui, W., Mizukami, H., Yanagisawa, M., Aida, T., Nomura, M., Isomura, Y., … Aizawa, H. (2014). Glial dysfunction in the mouse habenula causes depressive-like behaviors and sleep disturbance. *The Journal of Neuroscience*, *34*, 16273–16285.

Danbolt, N. C. (2001). Glutamate uptake. *Progress in Neurobiology*, *65*, 1–105.

Danbolt, N. C., Furness, D. N., & Zhou, Y. (2016). Neuronal vs glial glutamate uptake: Resolving the conundrum. *Neurochemistry International*, *98*, 29–45.

Durkee, C. A., & Araque, A. (2019). Diversity and specificity of astrocyte-neuron communication. *Neuroscience*, *396*, 73–78.

Eroglu, C., & Barres, B. A. (2010). Regulation of synaptic connectivity by glia. *Nature*, *468*, 223–231.

Espinosa, J. S., & Stryker, M. P. (2012). Development and plasticity of the primary visual cortex. *Neuron*, *75*, 230–249.

Felix, L., Stephan, J., & Rose, C. R. (2020). Astrocytes of the early postnatal brain. *The European Journal of Neuroscience*, 1–24.

Feng, G., Mellor, R. H., Bernstein, M., Keller-Peck, C., Nguyen, Q. T., Wallace, M., … Sanes, J. R. (2000). Imaging neuronal subsets in transgenic mice expressing multiple spectral variants of GFP. *Neuron*, *28*, 41–51.

Foxworthy, W. A., & Medina, A. E. (2015). Overexpression of serum response factor in neurons restores ocular dominance plasticity in a model of fetal alcohol Spectrum disorders. *Alcoholism, Clinical and Experimental Research*, *39*, 1951–1956.

Genoud, C., Quairiaux, C., Steiner, P., Hirling, H., Welker, E., & Knott, G. W. (2006). Plasticity of astrocytic coverage and glutamate transporter expression in adult mouse cortex. *PLoS Biology*, *4*, e343.

Gu, Y., & Cang, J. (2016). Binocular matching of thalamocortical and intracortical circuits in the mouse visual cortex. *eLife*, *5*, 1–14.

Hanson, E., Armbruster, M., Cantu, D., Andresen, L., Taylor, A., Danbolt, N. C., & Dulla, C. G. (2015). Astrocytic glutamate uptake is slow and does not limit neuronal NMDA receptor activation in the neonatal neocortex. *Glia*, *63*, 1784–1796.

Hauser, J. L., Edson, E. B., Hooks, B. M., & Chen, C. (2013). Metabotropic glutamate receptors and glutamate transporters shape transmission at the developing retinogeniculate synapse. *Journal of Neurophysiology*, *109*, 113–123.

Hensch, T. K. (2005). Critical period plasticity in local cortical circuits. *Nature Reviews. Neuroscience*, *6*, 877–888.

Herde, M. K., Bohmbach, K., Domingos, C., Vana, N., Komorowska-Muller, J. A., Passlick, S., … Henneberger, C. (2020). Local efficacy of glutamate uptake decreases with synapse size. *Cell Reports*, *32*, 108182.

Hooks, B. M., & Chen, C. (2020). Circuitry underlying experience-dependent plasticity in the mouse visual system. *Neuron*, *106*, 21–36.

Huang, Y. H., & Bergles, D. E. (2004). Glutamate transporters bring competition to the synapse. *Current Opinion in Neurobiology*, *14*, 346–352.

Huang, Y. H., Sinha, S. R., Tanaka, K., Rothstein, J. D., & Bergles, D. E. (2004). Astrocyte glutamate transporters regulate metabotropic glutamate receptor-mediated excitation of hippocampal interneurons. *The Journal of Neuroscience*, *24*, 4551–4559.

Ip, J. P. K., Nagakura, I., Petravicz, J., Li, K., Wiemer, E. A. C., & Sur, M. (2018). Major vault protein, a candidate gene in 16p11.2 microdeletion syndrome, is required for the homeostatic regulation of visual cortical plasticity. *Journal of Neuroscience*, *38*(16), 3890–3900.

Kara, P., & Boyd, J. D. (2009). A micro-architecture for binocular disparity and ocular dominance in visual cortex. *Nature*, *458*, 627–631.

Katz, L. C., & Crowley, J. C. (2002). Development of cortical circuits: Lessons from ocular dominance columns. *Nature Reviews. Neuroscience*, *3*, 34–42.

Kiryk, A., Aida, T., Tanaka, K., Banerjee, P., Wilczynski, G. M., Meyza, K., … Danysz, W. (2008). Behavioral characterization of GLT1 (+/−) mice as a model of mild glutamatergic hyperfunction. *Neurotoxicity Research*, *13*, 19–30.

Leamey, C. A., Van Wart, A., & Sur, M. (2009). Intrinsic patterning and experience-dependent mechanisms that generate eye-specific projections and binocular circuits in the visual pathway. *Current Opinion in Neurobiology*, *19*, 181–187.

Massie, A., Cnops, L., Jacobs, S., Van Damme, K., Vandenbussche, E., Eysel, U. T., … Arckens, L. (2003). Glutamate levels and transport in cat (*Felis catus*) area 17 during cortical reorganization following binocular retinal lesions. *Journal of Neurochemistry*, *84*, 1387–1397.

Matsugami, T. R., Tanemura, K., Mieda, M., Nakatomi, R., Yamada, K., Kondo, T., … Tanaka, K. (2006). From the cover: Indispensability of the glutamate transporters GLAST and GLT1 to brain development. *Proceedings of the National Academy of Sciences of the United States of America*, *103*, 12161–12166.

Muller, C. M., & Best, J. (1989). Ocular dominance plasticity in adult cat visual cortex after transplantation of cultured astrocytes. *Nature*, *342*, 427–430.

Murphy-Royal, C., Dupuis, J. P., Varela, J. A., Panatier, A., Pinson, B., Baufreton, J., … Oliet, S. H. (2015). Surface diffusion of astrocytic glutamate transporters shapes synaptic transmission. *Nature Neuroscience*, *18*, 219–226.

Nagakura, I., Van Wart, A., Petravicz, J., Tropea, D., & Sur, M. (2014). STAT1 regulates the homeostatic component of visual cortical plasticity via an AMPA receptor-mediated mechanism. *The Journal of Neuroscience*, *34*, 10256–10263.

Papouin, T., Dunphy, J., Tolman, M., Foley, J. C., & Haydon, P. G. (2017). Astrocytic control of synaptic function. *Philosophical Transactions of the Royal Society of London. Series B, Biological Sciences*, *372*, 1–8.

Perez-Alvarez, A., Navarrete, M., Covelo, A., Martin, E. D., & Araque, A. (2014). Structural and functional plasticity of astrocyte processes and dendritic spine interactions. *The Journal of Neuroscience*, *34*, 12738–12744.

Petr, G. T., Sun, Y., Frederick, N. M., Zhou, Y., Dhamne, S. C., Hameed, M. Q., … Rosenberg, P. A. (2015). Conditional deletion of the glutamate transporter GLT-1 reveals that astrocytic GLT-1 protects against fatal epilepsy while neuronal GLT-1 contributes significantly to glutamate uptake into synaptosomes. *The Journal of Neuroscience*, *35*, 5187–5201.

Pinky, N. F., Wilkie, C. M., Barnes, J. R., & Parsons, M. P. (2018). Region- and activity-dependent regulation of extracellular glutamate. *The Journal of Neuroscience*, *38*, 5351–5366.

Rikhye, R. V., & Sur, M. (2015). Spatial correlations in natural scenes modulate response reliability in mouse visual cortex. *The Journal of Neuroscience*, *35*, 14661–14680.

Robinson, M. B., Lee, M. L., & DaSilva, S. (2020). Glutamate transporters and mitochondria: Signaling, co-compartmentalization, functional coupling, and future directions. *Neurochemical Research*, *45*, 526–540.

Sato, M., & Stryker, M. P. (2008). Distinctive features of adult ocular dominance plasticity. *The Journal of Neuroscience*, *28*, 10278–10286.

Sawtell, N. B., Frenkel, M. Y., Philpot, B. D., Nakazawa, K., Tonegawa, S., & Bear, M. F. (2003). NMDA receptor-dependent ocular dominance plasticity in adult visual cortex. *Neuron*, *38*, 977–985.

Schafer, D. P., Lehrman, E. K., Kautzman, A. G., Koyama, R., Mardinly, A. R., Yamasaki, R., … Stevens, B. (2012). Microglia sculpt postnatal neural circuits in an activity and complement-dependent manner. *Neuron*, *74*, 691–705.

Schummers, J., Sharma, J., & Sur, M. (2005). Bottom-up and top-down dynamics in visual cortex. *Progress in Brain Research*, *149*, 65–81.

Singh, S. K., Stogsdill, J. A., Pulimood, N. S., Dingsdale, H., Kim, Y. H., Pilaz, L. J., … Eroglu, C. (2016). Astrocytes assemble Thalamocortical synapses by bridging NRX1alpha and NL1 via Hevin. *Cell*, *164*, 183–196.

Sipe, G. O., Lowery, R. L., Tremblay, M. E., Kelly, E. A., Lamantia, C. E., & Majewska, A. K. (2016). Microglial P2Y12 is necessary for synaptic plasticity in mouse visual cortex. *Nature Communications*, *7*, 10905.

Smith, G. B., Heynen, A. J., & Bear, M. F. (2009). Bidirectional synaptic mechanisms of ocular dominance plasticity in visual cortex. *Philosophical Transactions of the Royal Society of London. Series B, Biological Sciences*, *364*, 357–367.

Stevens, B., Allen, N. J., Vazquez, L. E., Howell, G. R., Christopherson, K. S., Nouri, N., … Barres, B. A. (2007). The classical complement cascade mediates CNS synapse elimination. *Cell*, *131*, 1164–1178.

Stowell, R. D., Sipe, G. O., Dawes, R. P., Batchelor, H. N., Lordy, K. A., Whitelaw, B. S., … Majewska, A. K. (2019). Noradrenergic signaling in the wakeful state inhibits microglial surveillance and synaptic plasticity in the mouse visual cortex. *Nature Neuroscience*, *22*, 1782–1792.

Sugimoto, J., Tanaka, M., Sugiyama, K., Ito, Y., Aizawa, H., Soma, M., … Tanaka, K. (2018). Region-specific deletions of the glutamate transporter GLT1 differentially affect seizure activity and neurodegeneration in mice. *Glia*, *66*, 777–788.

Takasaki, C., Okada, R., Mitani, A., Fukaya, M., Yamasaki, M., Fujihara, Y., … Watanabe, M. (2008). Glutamate transporters regulate lesion-induced plasticity in the developing somatosensory cortex. *The Journal of Neuroscience*, *28*, 4995–5006.

Takatsuru, Y., Iino, M., Tanaka, K., & Ozawa, S. (2007). Contribution of glutamate transporter GLT-1 to removal of synaptically released glutamate at climbing fiber-Purkinje cell synapses. *Neuroscience Letters*, *420*, 85–89.

Tanaka, K., Watase, K., Manabe, T., Yamada, K., Watanabe, M., Takahashi, K., … Wada, K. (1997). Epilepsy and exacerbation of brain injury in mice lacking the glutamate transporter GLT-1. *Science*, *276*, 1699–1702.

Tie, X., Li, S., Feng, Y., Lai, B., Liu, S., & Jiang, B. (2018). Distinct roles of NMDAR and mGluR5 in light exposure reversal of feedforward synaptic strength in V1 of juvenile mice after binocular vision deprivation. *Neuroscience*, *384*, 131–138.

Trachtenberg, J. T. (2015). Competition, inhibition, and critical periods of cortical plasticity. *Current Opinion in Neurobiology*, *35*, 44–48.

Verkhratsky, A., & Nedergaard, M. (2018). Physiology of Astroglia. *Physiological Reviews*, *98*, 239–389.

Voutsinos-Porche, B., Knott, G., Tanaka, K., Quairiaux, C., Welker, E., & Bonvento, G. (2003). Glial glutamate transporters and maturation of the mouse somatosensory cortex. *Cerebral Cortex*, *13*, 1110–1121.

Wang, B. S., Sarnaik, R., & Cang, J. (2010). Critical period plasticity matches binocular orientation preference in the visual cortex. *Neuron*, *65*, 246–256.

Weng, H. R., Chen, J. H., Pan, Z. Z., & Nie, H. (2007). Glial glutamate transporter 1 regulates the spatial and temporal coding of glutamatergic synaptic transmission in spinal lamina II neurons. *Neuroscience*, *149*, 898–907.

Zhou, J., & Sutherland, M. L. (2004). Glutamate transporter cluster formation in astrocytic processes regulates glutamate uptake activity. *The Journal of Neuroscience*, *24*, 6301–6306.

How to cite this article: Sipe GO, Petravicz J, Rikhye RV, Garcia R, Mellios N, Sur M. Astrocyte glutamate uptake coordinates experience-dependent, eye-specific refinement in developing visual cortex. *Glia*. 2021;69:1723–1735. https://doi.org/10.1002/glia.23987